BNL-225264-2024-JAAM

Kinetics of simultaneous hydrodesulfurization and hydrodenitrogenation reactions using CoMoP/Al2O3 and NiMoP/Al2O3

G. de Souza Guedes Junior, J. Boscoboinik

To be published in "Chemical Engineering Science"

July 2023

Center for Functional Nanomaterials

Brookhaven National Laboratory

U.S. Department of Energy

USDOE Office of Science (SC), Basic Energy Sciences (BES). Scientific User Facilities (SUF)

DISCLAIMER

Kinetics of simultaneous hydrodesulfurization and hydrodenitrogenation reactions using $CoMoP/Al_2O_3$ and $NiMoP/Al_2O_3$

Gentil de Souza Guedes Junior[a], Idia Gigante Nascimento[a], Mueed Ahmad[b,c], Cormac Killeen[b], J.Anibal Boscoboinik[c], Jason Trelewicz[b,d], José Carlos Pinto[e], Matheus Dorneles de Mello[a,c], Mônica Antunes Pereira da Silva[a*],

[a]*Escola de Química, Universidade Federal do Rio de Janeiro, Rio de Janeiro, Brazil, 21949-900.* [*]*e-mail: monica@eq.ufrj.br*

[b]*Department of Materials Science and Chemical Engineering, Stony Brook University, Stony Brook, New York 11794, United States*

[c]*Center for Functional Nanomaterials, Brookhaven National Laboratory, Upton, New York 11973, United States*

[d]*Institute for Advanced Computational Science, Stony Brook University, Stony Brook, New York 11794, United States*

[e]*Programa de Engenharia Química/COPPE, Universidade Federal do Rio de Janeiro, Cidade Universitária, - CP: 68502, Rio de Janeiro, RJ, 21941-972,*

ABSTRACT

Hydrodesulfurization (HDS) is a key reaction to achieve diesel production at the specified low sulfur levels and is highly affected by a competing reaction involving nitrogen removal through hydrodenitrogenation (HDN). This work evaluated kinetic parameters of simultaneous reactions of HDS of dibenzothiophene (DBT) and HDN of quinoline (Q) using $CoMoP/Al_2O_3$ and $NiMoP/Al_2O_3$ catalysts under operational conditions that allow a wide range of reagent conversions. Estimated parameters were evaluated using rigorous statistical

analysis. Good fits for the evaluated experimental data were provided by both power-law and Langmuir-Hinshelwood models. Turnover frequency values highlight adsorption and competition effects between nitrogen-containing compounds and sulfur-containing compounds. NiMoP catalyst showed higher hydrogenating power than CoMoP, with larger absolute value of the estimated adsorption enthalpy (-120 kJ.mol^{-1} for NiMoP and -75 kJ.mol^{-1} for CoMoP), suggesting strong adsorption of nitrogen compounds. A catalyst with more hydrogenating power is also more capable of performing both HDN and HDS reactions simultaneously.

Keywords: Dibenzothiophene; quinoline; CoMoP/Al_2O_3; NiMoP/Al_2O_3; kinetic modeling; statistical analysis; deep hydrodesulfurization

1. Introduction

In recent decades, the importance of processes that convert heavy petroleum fractions into lighter and cleaner products has been emphasized because of increasing environmental concerns and more strict specifications for oil-based fuels [1–3]. In this regard, the removal of contaminants such as sulfur and nitrogen through hydrotreatment (HDT) constitutes an essential step that precedes processes such as reforming and catalytic cracking [4]. However, the performance of the process regarding the various reactions, such as hydrodesulfurization (HDS) and hydrodenitrogenation (HDN), is linked to the type of catalyst and reactor employed [5].

The most used catalysts in HDT processes are molybdenum sulfides, promoted by nickel or cobalt [6,7]. Generally, these catalysts are supported on refractory oxides, and alumina is the most used one [8]. It is accepted that there are two types of active sites in these supported catalysts: coordinately unsaturated sites (CUS) and hydrogenation ones [9]. Girgis and Gates [10] showed that catalysts promoted by nickel display higher activity at hydrogenation sites when compared to catalysts promoted by cobalt. Additives (such as phosphorus) are also used to increase the catalytic activity due to enhanced active metal sulfide phase dispersion [11–15].

HDS reactions of different compounds, including dibenzothiophenes and their substituents, have been studied by several groups [16–19]. It is generically accepted that dibenzothiophene (DBT) reacts by two routes: (i) direct desulfurization (DDS) through the breaking of C-S bonds, leading to the formation of biphenyl; and (ii) hydrogenation of one of the benzene rings (HYD) followed by desulfurization, forming cyclohexylbenzene (CHB) and dicyclohexyl (DCH) [20–27]. Figure 1A shows DBT reaction pathways.

The reaction scheme of HDN is more complex and involves more reaction steps [28,29]. Jian and Prins [30] studied the HDN reaction of quinoline on a NiMoP/Al_2O_3 catalyst

and stated that the reactions occur in three steps: (i) the hydrogenation of aromatic heterocyclic rings; (ii) the cleavage of the C-N bond; and (iii) the hydrogenation of the benzene rings. Figure 1B illustrates quinoline reaction pathways.

Kinetic modeling of HDS and HDN reactions can be a powerful tool for selecting and developing catalysts, reactor design, and catalyst deactivation studies [31–50]. Most efforts have been devoted to modeling HDS reactions, including the proposition of reaction schemes and estimation of kinetic and thermodynamic parameters, such as the apparent activation energies of reaction steps and enthalpy of adsorption of compounds [33–35,48–50]. In parallel, the increased use of heavier feedstocks with nitrogen-containing molecules has led to larger number of studies on the kinetics of HDN reactions [36–39,51]. However, due to the complexity of the reaction schemes, few studies address the modeling of HDS and HDN reactions simultaneously [41,42,52–59]. In this case, the models used most often to determine kinetic parameters are Power Law (PL) models [54–57,60,61] and Langmuir-Hinshelwood (LH) models [57–59,62]. LH models consider the adsorption of reactants and products on the surfaces of the catalyst. This way, these models can describe the effects of competition among distinct molecules for active sites. However, the estimation of parameters in these models is more challenging, as the resulting mathematical structure leads to strongly correlated model parameters [63]. In contrast, although PL models cannot provide information regarding the competition and inhibition effects exerted by distinct molecules, such models are usually preferred in industrial environments to represent the reaction kinetics due to their simplicity in analyzing complex reaction schemes [64].

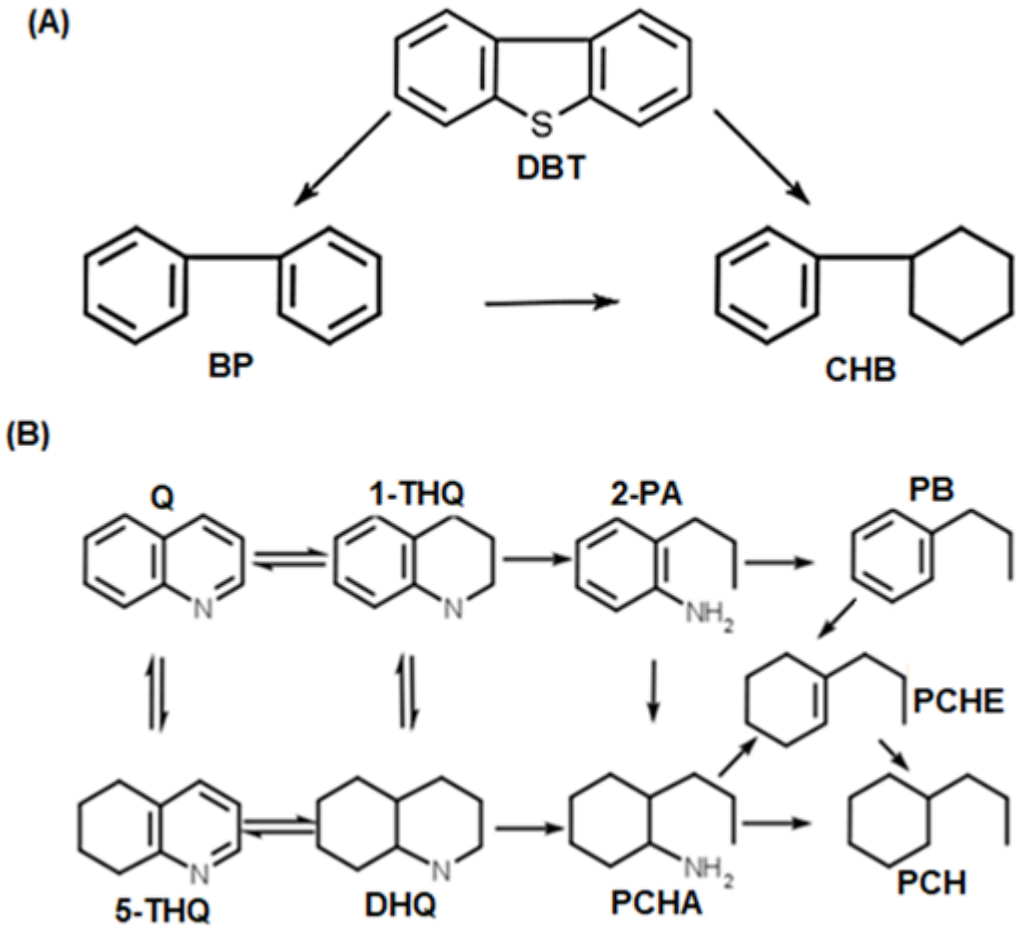

Figure 1. Reaction pathways for HDS of dibenzothiophene (A) and HDN of quinoline (B).

Moreover, it is important to emphasize that the quality of experimental data, the lack of obvious search limits for parameter estimates in the parameter search space, and the lack of generical modeling tools that can describe a wide range of kinetic models are additional difficulties that characterize the challenge of estimating accurate kinetic parameters in most actual problems [65–68].

Despite extensive previous studies on modeling hydrotreating reactions, estimation of kinetic parameters that take into account the statistical rigor of the experimental data and the parameter estimation procedure are relatively rare in the literature. Furthermore, it is not common to correlate the kinetic parameters with the physicochemical properties of the

catalyst. These important literature gaps encouraged the investigation and modeling of the kinetics of simultaneous HDS and HDN reactions using NiMoP and CoMoP catalysts. In order to do that, new experimental data are collected in a continuous flooded fixed-bed reactor at a broad set of operating conditions. Then, PL and LH kinetic models were proposed and examined, considering the actual experimental errors during the estimation of kinetic parameters. Finally, the parameters were evaluated and validated for their physical and statistical significance.

2. Experimental

2.1. Catalyst Preparation and Characterization

The CoMoP and NiMoP catalysts were prepared by the incipient wetness impregnation technique, using calcined Pural SB alumina as support. The catalyst contained 20 % (m/m) of MoO_3, and the atomic ratio Ni(Co)/(Ni(Co)+Mo) was equal to 0.3. The P/Mo atomic ratio was set to 0.4 for both catalysts. A detailed description of the preparation steps can be found in Nascimento et al. [64]. The catalysts CoMoP/Al_2O_3 and NiMoP/Al_2O_3 are referred to CoMoP and NiMoP, respectively. The catalysts were characterized in their oxide form previously. X-Ray Photoelectron Spectroscopy (XPS) and Transmission Electron Microscopy (HRTEM) of the sulfided materials were added here for completion. The particle sizes of catalysts used to perform the reactions ranged between 0.150 and 0.250 mm.

a) XPS

X-ray photoelectron spectroscopy (XPS) spectra of sulfided NiMoP/Al_2O_3 and CoMoP/Al_2O_3 powders were collected at room temperature and under UHV (base pressure of 10^{-9} mbar) using a SPECS electron spectrometer system equipped with PHOIBOS NAP 150 hemispherical energy analyzer and a monochromatic Al Kα X-ray source (1486.7 eV). The powdered samples were pressed on copper tape mounted on a stainless-steel flag-type

sample holder. The charging effect was compensated using an electron gun equipped with the XPS system. Components Co 2p and Ni 2p were collected with 25 scans for a better signal to noise ratio. C 1s spectra corresponding to adventitious carbon were used as a reference for further calibration at 284.8 eV.

b) HRTEM

High-resolution transmission electron microscopy (HRTEM) images were taken on a JEOL 2100F instrument with a point-to-point resolution of 2.3 Å in TEM mode using an accelerating voltage of 200 keV. Statistical analyses of the lengths and stacking layer numbers of 200 slabs were carried out according to Eq. (1), where the average slab length (L) and stacking number (N) were calculated [69] by:

$$L(\text{or } N)=\frac{\sum_{i=1}^{n} x_i M_i}{\sum_{i=1}^{n} x_i} \quad (1)$$

where M_i is the measured property of a stacked MoS_2 unit, and x_i is the number of slabs or stacks in that range. Mo dispersion (f_{Mo}) was also obtained out of the TEM micrographs according to Eq. (2) by dividing the total number of Mo atoms located at the edge surface (Mo_{edge}) by the total number of Mo atoms (Mo_{total}) [70], in the form:

$$f_{Mo}=\frac{Mo_{edge}}{Mo_{total}}=\frac{\sum_{i=1}^{t}(6n_i-6)}{\sum_{i=1}^{t}(3n_i^2-3n_i+1)} \quad (2)$$

where $n_i$is the number of Mo atoms along the edge of a MoS_2 slab determined from its length 1 ($L=3.2(2n_i-1)$) Å), and t is the total number of slabs determined from HRTEM images of a 20 sulfided catalyst [71]. In this test, t was always equal to 200.

2.2. Reaction System

HDS of DBT (Sigma-Aldrich, 98 %) and HDN of quinoline (Sigma-Aldrich, 96 %) were carried out in a flooded-bed reactor (Micro Activity-Reactor Reference, provided by PID Eng & Tech), operating in upflow mode under different conditions. In a typical trial, about 0.57 g of catalyst in the oxide form (60-100 mesh) was placed in the central zone of the reactor and diluted with 0.75 g of silicon carbide. The initial reaction load was composed of 3500 mg kg^{-1} of S with varying concentration of quinoline. The solvent used was n-hexadecane (C_{16}, Sigma-Aldrich, 99 %). The specific mass of the feed was equal to 0.773 g. cm^{-3}. Before the reaction, the catalysts were sulfided *in situ* in two steps using a solution containing 4 wt% of CS_2 and n-hexane (0.10 mL. min^{-1}). The first stage of sulfidation was performed at 250 °C for 120 min, and the second was conducted at 350 °C for 180 min. The heating rate was set to 2°C.min^{-1}. Reaction samples were collected periodically and analyzed with an Agilent Gas Chromatograph (7820A model), using a flame ionization detector and a DB-1 capillary column (60 m long, with 0.32 mm of inner diameter and 0.5 μm of film thickness).

2.3. Catalyst Tests

The experiments were performed at temperatures between 240 and 340 °C, while the H_2 pressure was kept at 60 bar, the weight hourly space velocity (WHSV) ranged between 14 and 30 h^{-1}, and the concentration of N from quinoline in the feed ranged from 150 to 450 mg.kg^{-1} N. The gas/feed ratio was kept constant at 400 (NL. L^{-1}). The hydrogen concentration in the liquid phase was estimated with HYSYS by a flash calculation using the Soave-Redlich-Kwong equation of state [72]. The experimental error was evaluated from replicates obtained at a specific set of reaction conditions for each of the catalysts. A load of 150 mg.kg^{-1} of N was used as the replicate condition for both catalysts. For NiMoP, the

replicate condition was set to 280 °C and 22 h^{-1}, while the condition at 310 °C and 16 h^{-1} was used for the cobalt catalyst. Different experimental conditions were selected to achieve isoconversion conditions for both materials. This difference in conditions was necessary due to the low concentrations of non-nitrogen compounds found in the cobalt-promoted catalyst at 280 °C at 22 h^{-1}.

2.4. Estimation of Kinetic Parameters

Parameter estimation was performed with a hybrid numerical procedure that combines a heuristic and a deterministic method. The heuristic method was based on particle swarm optimization (PSO). The PSO is an efficient algorithm for the global minimization of the maximum likelihood objective function, presented in the form of the weighted least squares function, using the inverse of the experimental variances as weights [73]. As the search for the minimum value of the objective function is stochastic and does not use the Hessian matrix of second derivatives, the probability of finding the global minimum is greater than other deterministic methods [73]. One thousand iterations and 100 particles were used to perform the PSO. The parameters that consider the individual and group contributions to the speed of each particle were equal to 1.5, and the factor of inertia was equal to 0.75 [73]. The tolerances adopted for the model parameters and the objective function were equal to 10^{-10} and 10^{-8}, respectively. The selected deterministic method was the well-known Gauss-Newton procedure for estimating the parameters of PL models and the Nelder-Mead algorithm for estimating the parameters of LH models and avoiding the computation of derivatives [74,75].

The adequacy of the obtained models was tested with the help of correlation coefficients (R) and the chi-square test. The confidence intervals of the model parameters were obtained with the t-Student distribution for PL models and the Fisher–Snedecor

distribution for LH models with a confidence level of 95 %. Parameter correlations were also evaluated to examine the strength of the association between pairs of model parameters [63].

In their usual forms, the mathematical structure of the Arrhenius and van't Hoff equations introduce a high correlation between pre-exponential parameters and activation energy (or heat of adsorption). This fact makes even more difficult to estimate the correct values of the model parameters. To circumvent this problem, the reparametrization of the Arrhenius and van't Hoff equations were proposed, introducing a reference temperature as shown below [76]:

$$k_i\ (K_i) = e^{\left(-a_i + b_i\left(1 - \frac{T_{ref}}{T}\right)\right)} \quad (3)$$

$$E_i\ (\Delta H_i) = R T_{ref} b_i \quad (4)$$

$$\ln k_{0,i}\ (\ln K_{0,i}) = e^{(b_i - a_i)} \quad (5)$$

where E_i and $\Delta H_{ads,j}$ are the apparent activation energy of reaction i and adsorption enthalpy of j, respectively, expressed in J mol^{-1}; R is the universal ideal gas constant in J K^{-1}; T and T_{ref} are, respectively, the temperature and the reference temperature, in K; $\ln k_{0,i}$ and $\ln K_{0,j}$ are the logarithms of the pre-exponential factor of the approval of Arrhenius and van't Hoff and a_i, b_i, a_j and b_j are model parameters to be estimated. This reparameterization was reported previously by Schwaab et al. (2008) [76].

Initially, the reference temperature was calculated as the average temperature of the experiments. However, an attempt was made to minimize the correlation between parameters a_i and b_i through optimization. In order to do that, a standard objective function described in Equation (6) was defined to reduce the degree of correlation between each pair of parameters. The optimization of the reference temperatures, therefore, can be performed through the minimization of the proposed standard form [76]:

$$N=\sum_{i=1}^{NP-1}\sum_{j=i+1}^{NP}\rho_{ij}^{2} \quad (6)$$

where NP is the number of model parameters, ρ_{ij} is the correlation between parameters i and j, and N is the norm to be minimized. The equations used for calculation of the correlation between parameters i and j are available in Supplementary Material (Section S4).

3. Results and Discussion

3.1. Characterization Analyses

Mo 3d, Ni 2p and Co 2p XPS profiles corresponding to sulfided CoMoP and NiMoP catalysts are presented in Figure 2. Mo signals were fitted considering doublets (corresponding to $3d_{5/2}$ and $3d_{3/2}$ contributions) due to Mo^{6+} (MoO_x), Mo^{5+} (MoO_xS_y) and Mo^{4+} (MoS_2) species with a characteristic separation of 3.2 eV and ratio between spin-orbit doublet of 0.66. Mo $3d_{5/2}$ peak for the first set, at 229.0 eV, was assigned to MoS_2 (Mo^{4+}); at 232.0 eV was attributed to Mo^{6+}; and other at 230.0 eV was associated with MoS_xO_y (Figures 2 (A) and 2 (C)) [77]. Meanwhile, the S 2s (226.8 eV) area was deducted.

Regarding Ni (Figure 2 (B)) species, the Ni 2p envelope of the NiMoP catalyst was decomposed by considering three major contributions, namely NiS_x (including Ni_3S_2, Ni_9S_8 or NiS, with binding energy 852.5 eV), oxidic nickel (binding energy ~856.7 eV) and NiMoS phase (binding energy 854.4 eV). As the energetic resolution of the XPS could hardly allow the correct decomposition of Ni signals, only the contribution from Ni $2p_{3/2}$ was used in the fit. Thus, the nickel species analyses should be considered semiquantitatively [78].

The fitting of the Co 2p region for catalyst CoMoP (Figure 2 (D)) was also done as already described for the Ni 2p region. In this case, the spectrum displayed primary satellite peaks due to shake-up electrons in addition to the main contribution from the Co $2p_{3/2}$. Each Co $2p_{3/2}$ profile was resolved in three components at 783.0, 780.1 and 785.3 eV, corresponding to highly dispersed Co_9S_8, CoMoS and CoO_x phases, respectively [79].

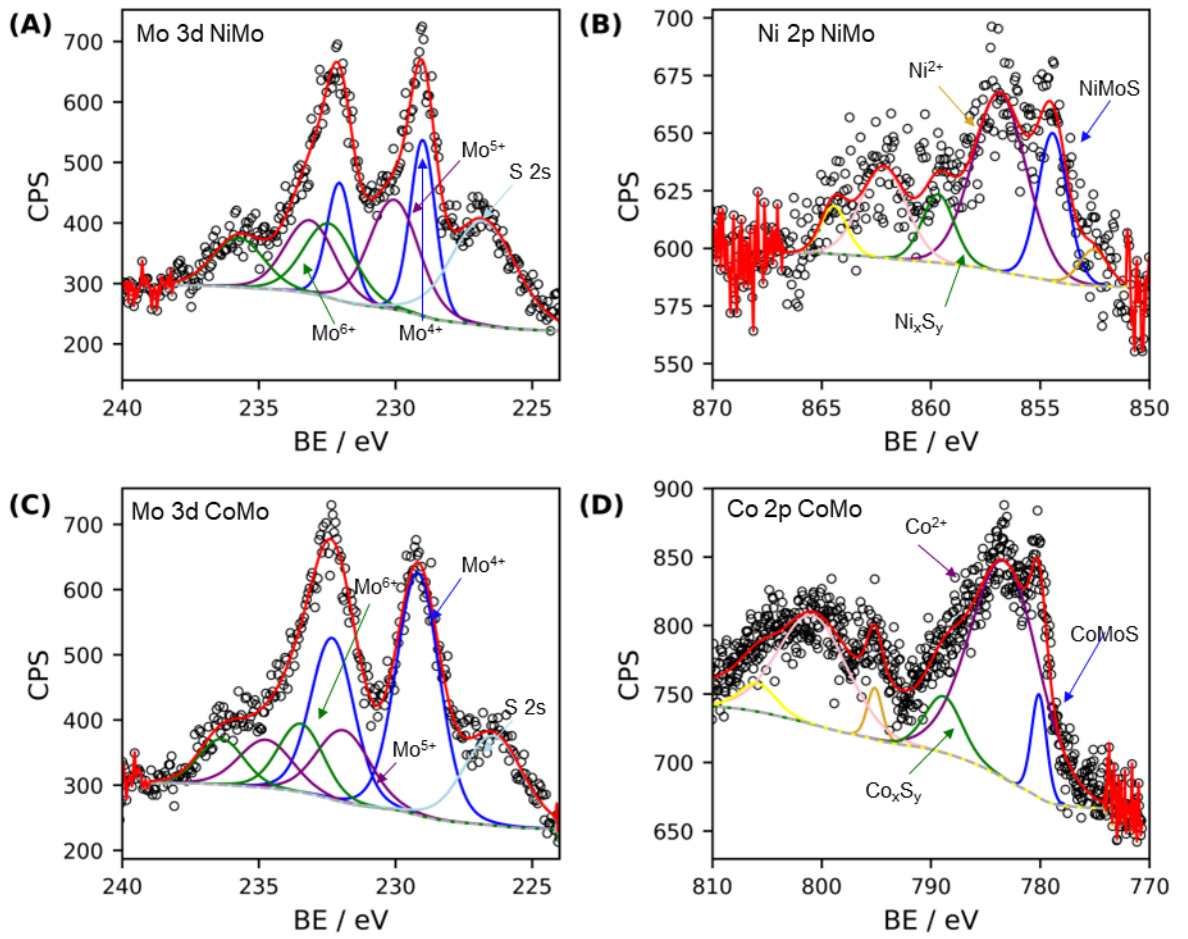

Figure 2. XPS profiles corresponding to sulfided CoMoP and NiMoP catalysts: (A) Mo 3d region of catalyst NiMoP; (B) Ni 2p region of catalyst NiMoP; (C) Mo 3d region of catalyst CoMoP; (D) Co 2p region of catalyst CoMoP. Colors in parts (A) and (C): Blue - Mo^{4+}; purple – Mo^{5+}; green – Mo^{6+}, and light blue – S 2s. Colors in parts (B) and (D): Blue – NiMoS/CoMoS; purple – Ni^{2+}/ Co^{2+}; green – Ni_xS_y/Co_xS_y, and pink and yellow – satellite peaks.

The amount of each species on the catalyst surface can be quantified as the ratio between the area of an element and the respective sensitivity factor, according to Eq. (7):

$$\frac{n_a}{n_b} = \frac{\frac{A_a}{S_a}}{\frac{A_b}{S_b}} \quad (7)$$

where n_a and n_b are the amounts of species a and b, respectively; A_a and A_b are the measured areas of the species a and b; S_a and S_b are the sensitivity factors of the atom related to the species a and b, respectively.

The concentration of the Al 2s region was normalized and the data are summarized in Table 1. As one can see, most sulfided Mo species exist in both catalysts. However, catalyst CoMoP exhibited more sulfided species than NiMoP, which is due to a higher Mo content from the synthesis and agrees with ICP results obtained by Nascimento et al. (2021) [64]. A significant amount of Ni and Co in oxide form suggests some oxidation of the samples, probably between sulfidation and the characterization. The degree of promotion (DP) was calculated by taking the ratio of NiMoS (or CoMoS) species by Mo^{4+} species (Eq. (8)). The data showed the enhancement of decorated MoS_2 slabs with Ni in NiMoP catalyst than with Co in CoMoP catalyst, which suggests the formation of more hydrogenating and active sites, according to the literature [15].

Table 1. Ni and Mo atomic concentration ratios and degree of promotion (DP) of NiMoP and CoMoP catalysts.

Catalyst	**Mo 3d**			**Ni 2p** **Co 2p**			**P/Al**	**DP (%)**
	Mo^{4+}/Al	Mo^{5+}/Al	Mo^{6+}/Al	NiS/Al CoS/Al	NiMoS/Al CoMoS/Al	Ni^{2+}/Al Co^{2+}/Al		
NiMoP	0.030	0.037	0.020	0.001	0.004	0.008	0.06	13.30
CoMoP	0.073	0.027	0.048	0.003	0.006	0.005	0.03	8.20

$$\frac{Ni}{Mo} = \frac{[NiMoS]}{[Mo^{4+}]} \quad (8)$$

Figure 3 shows HRTEM micrographs of the sulfided NiMoP and CoMoP catalysts. Black thread-like fringes correspond to MoS_2 slabs with different stack heights and lengths on the Al_2O_3 surface. The statistical results on the length and stacking distributions can be found in Table 2. According to the TEM results, the average slab lengths and stacking numbers were similar for both catalysts, even though the distribution was slightly shifted towards smaller slabs for NiMoP, when compared to CoMoP. The degree of Mo dispersion of the slabs was determined by considering that only the edge of MoS_2 slabs exhibited catalytic activity [80]. NiMoP displayed the dispersion of 0.30, while CoMoP displayed the dispersion of 0.33. The similarity in length, stacking and dispersion suggests unremarkable changes in the catalyst micromorphology.

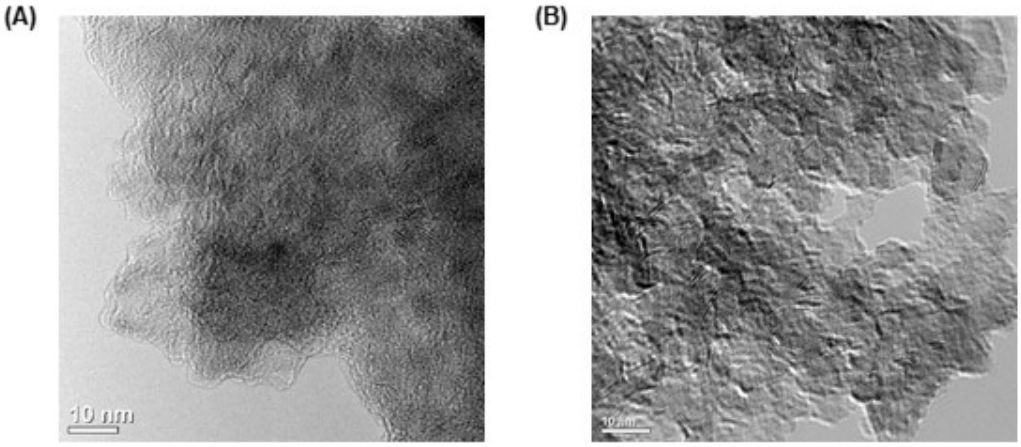

Figure 3. HRTEM micrographs of CoMoP (A) and NiMoP (B) sulfide catalysts.

Table 2. HRTEM results for NiMoP and CoMoP sulfide catalysts.

	NiMoP	CoMoP
Relative frequency for slab length (%)		
< 2 nm	8	0
2 – 3 nm	31	27
3 – 4 nm	32	31
4 – 5 nm	17	30
5 – 6 nm	10	11
> 6 nm	2	1
Relative frequency for stacking layers (%)		
1	12	27
2	42	26
3	35	26
4	13	14
>4	4	7
Average slab length, nm	3.6	3.7
Average stacking layers	1.9	1.9
Dispersion degree of Mo species	0.3	0.33

5

3.2. Effects on Conversion and Product Yields

The effects of temperature, WHSV and initial quinoline concentration on DBT and HDN conversions and product yields are shown in Figure 4. Y_N and Y_{NN} are, respectively, the yield in nitrogenous and non-nitrogenous compounds. As expected, the increase in temperature favored the conversion of DBT and HDN for both catalysts (Figures 4 (A), (E), (I), (M)) [81]. Reaction temperatures below 280 °C resulted in low conversions to non-nitrogenated products, indicating the strong adsorption of quinoline and its nitrogen-containing intermediates on the active sites [11,82]. Increasing WHSVs reduced conversions and yields in HDS and HDN products for both catalysts, as expected (Figures 4 (B), (F), (J), (N)). However, the overall yield to non-HDN products increased with a shorter contact time between the reactants and the active sites of the catalyst. Changing the initial nitrogen concentration also affected the HDS and HDN conversions. An increase in Q concentration resulted in the decrease of DBT and HDN conversions (Figures 4 (C), (D), (G), (H), (K), (L), (O), (P)), which constitutes evidence of strong adsorption of nitrogen containing intermediates on the active sites of the catalysts [83,84]. Under similar reaction conditions, NiMoP catalyst showed higher HDN conversions than CoMoP, supporting reports that indicate that Ni catalysts show superior hydrogenating power than Co ones [10].

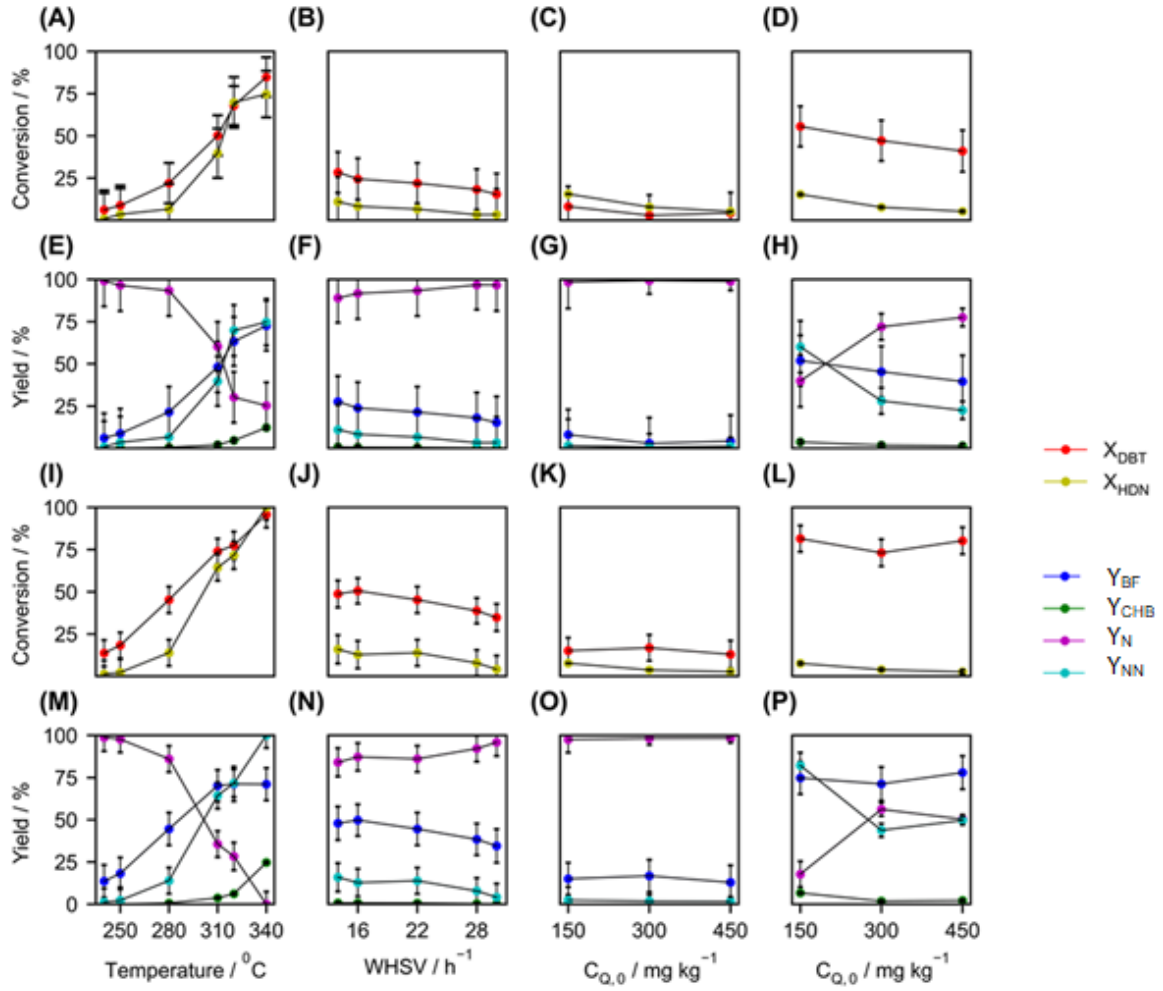

Figure 4. Effects of process variables on the DBT HDS and Q HDN conversion and product yields for catalysts CoMoP (Panels (A) to (H)) and NiMoP (Panels (I) to (P)). Temperature: (A), (E), (I) and (M) evaluated at 22 h^{-1} and 150 $mg.kg^{-1}$ N. WHSV: (B), (F), (J), (N) evaluated at 280 °C and 150 $mg.kg^{-1}$ N. $C_{Q,0}$: (C), (G), (K) and (L) evaluated at 250 °C and 28 h^{-1} and (D), (H), (L) and (P) evaluated at 310 °C and 16 h^{-1}.

3.3. Kinetic Modeling of the Experimental Data

For purposes of reactor modeling, the differential mass balance equations can be written in the form of Eq. 9:

$$\frac{dC_j}{d\tau} = \rho r_j \quad (9)$$

considering steady state conditions, isothermal and isobaric operation, plug flow regime without existence of radial concentration gradients, one-dimensional model, and constant volume flow.

For purposes of kinetic modeling, the reaction scheme assumed that DBT reacts through two routes: DDS and HYD, forming BP and CHB, respectively. Due to its complexity, the HDN reaction was simplified to convert the nitrogen-containing compounds directly to denitrogenated species. This approach was adopted in this work given the complexity of quinoline's reaction network and many parameters involved in the reaction scheme, reducing the number of degrees of freedom and making the estimation difficult. Furthermore, it was a strategy used by Novaes et al. (2015b) [52] when working with real feedstocks. In that work, the HDN was modeled with a power law model. According to this proposal, the concentration of molecules without nitrogen is equivalent to the sum of concentrations of PCH, PCHE, and PB. Initially, the nitrogen concentration comes only from quinoline. The nitrogen concentration at steady state is the difference between the initial nitrogen concentration and the concentration of formed nitrogen-containing intermediates.

Moreover, the kinetic modeling assumed that: (i) surface reaction is the limiting step of the process; (ii) there is only one type of active site; (iii) non-dissociative hydrogen adsorption; (iv) irreversible and liquid-phase reactions; (v) negligible inhibitory effect caused by NH_3 and H_2S molecules due to low concentrations in a liquid medium; (vi) constant hydrogen concentration; (vii) preponderant adsorption constant of nitrogenous compounds compared to the others; (viii) total active sites, kinetic constant, reagent adsorption constants, and hydrogen concentration encompassed in a single constant κ. Under such hypotheses, a

phenomenological model, LHI, and an empirical one, LPI, can be proposed, as well as models that consider only the consumption of reagent species, LHG and LPG, respectively, and their 3 results are shown in Table 3.

Table 3. Estimated parameters and statistics for simultaneous DBT HDS and Q HDN on CoMoP and NiMoP catalysts with different modeling approaches.

Model	Equation	CoMoP		NiMoP	
		Parameter	Statistical metrics	Parameter	Statistical metrics
LPG	$\frac{dC_{DBT}}{d\tau}=-\rho k_1 C_{DBT}$ $\frac{dC_N}{d\tau}=-\rho k_2 C_N$	$E_1 = 108.7 \pm 17.7$ $\ln k_{0,1} = 26.2 \pm 3.6$ $T_{ref,1} = 564$ $E_2 = 468.8 \pm 114.4$ $\ln k_{0,2} = 98.6 \pm 23.6$ $T_{ref,2} = 579$	$\chi^2_{min} = 24.4$ $\chi^2_{max} = 59.3$ $F_{obj} = 96.5$ $n_p = 4$ $AIC_c = 1.2$	$E_1 = 84.3 \pm 7.2$ $\ln k_{0,1} = 20.9 \pm 1.5$ $T_{ref,1} = 581$ $E_2 = 150.5 \pm 13.4$ $\ln k_{0,2} = 33.8 \pm 2.8$ $T_{ref,2} = 584$	$\chi^2_{min} = 24.4$ $\chi^2_{max} = 59.3$ $F_{obj} = 199.7$ $n_p = 4$ $AIC_c = -0.2$
LPI	$\frac{dC_{DBT}}{d\tau}=-\rho k_1 C_{DBT}-\rho k_2 C_{DBT}$ $\frac{dC_{BP}}{d\tau}=\rho k_1 C_{DBT}$ $\frac{dC_{CHB}}{d\tau}=\rho k_2 C_{DBT}$ $\frac{dC_N}{d\tau}=-\rho k_3 C_N$ $\frac{dC_{NN}}{d\tau}=\rho k_3 C_N$	$E_1 = 92.5 \pm 11.8$ $\ln k_{0,1} = 21.9 \pm 2.4$ $T_{ref,1} = 562$ $E_2 = 229.7 \pm 22.8$ $\ln k_{0,2} = 47.1 \pm 4.5$ $T_{ref,2} = 583$ $E_3 = 468.1 \pm 84.8$ $\ln k_{0,3} = 98.5 \pm 17.5$ $T_{ref,3} = 579$	$\chi^2_{min} = 77.7$ $\chi^2_{max} = 134.1$ $F_{obj} = 218.0$ $n_p = 6$ $AIC_c = 6.8$	$E_1 = 50.5 \pm 3.9$ $\ln k_{0,1} = 13.6 \pm 0.8$ $T_{ref,1} = 579$ $E_2 = 274.8 \pm 6.7$ $\ln k_{0,2} = 56.7 \pm 1.4$ $T_{ref,2} = 603$ $E_3 = 173.8 \pm 13.9$ $\ln k_{0,3} = 38.6 \pm 2.9$ $T_{ref,3} = 584$	$\chi^2_{min} = 77.7$ $\chi^2_{max} = 134.1$ $F_{obj} = 1223$ $n_p = 6$ $AIC_c = 3.4$
LHG	$\frac{dC_{DBT}}{d\tau}=\frac{-\rho\kappa_1 C_{DBT}}{(1+K_N C_N)^2}$ $\frac{dC_N}{d\tau}=\frac{-\rho\kappa_2 C_N}{(1+K_N C_N)^2}$	$E_1 = 53.3 \pm 36.6$ $\ln \kappa_{0,1} = 14.6 \pm 7.3$ $T_{ref,1} = 565$ $E_2 = 108.2 \pm 35.9$ $\ln \kappa_{0,2} = 25.4 \pm 7.2$ $T_{ref,2} = 583$ $\Delta H_{ads,N} = 56.5 \pm 45.2$ $\ln K_{N,0} = -7.8 \pm 9.3$ $T_{ref,3} = 553$	$\chi^2_{min} = 22.9$ $\chi^2_{max} = 56.9$ $F_{obj} = 34.7$ $n_p = 6$ $AIC_c = 10.5$	$E_1 = 85.0 \pm 15.8$ $\ln \kappa_{0,1} = 21.2 \pm 3.3$ $T_{ref,1} = 582$ $E_2 = 146.4 \pm 18.2$ $\ln \kappa_{0,2} = 33.0 \pm 18.2$ $T_{ref,2} = 603$ $\Delta H_{ads,N} = 26.4 \pm 218.7$ $\ln K_{N,0} = -7.0 \pm 45.2$ $T_{ref,2} = 553$	$\chi^2_{min} = 22.9$ $\chi^2_{max} = 56.9$ $F_{obj} = 196.0$ $n_p = 6$ $AIC_c = 7.0$

Table 3. Estimated parameters and statistics for simultaneous DBT HDS and Q HDN on CoMoP and NiMoP catalysts with different modeling approaches (cont.)

Model	Equation	CoMoP		NiMoP	
		Parameter	Statistical metrics	Parameter	Statistical metrics
LHI	$\frac{dC_{DBT}}{d\tau}=\frac{-\rho\kappa_1 C_{DBT}-\rho\kappa_2 C_{DBT}}{(1+K_N C_N)^2}$ $\frac{dC_{BP}}{d\tau}=\frac{\rho\kappa_1 C_{DBT}}{(1+K_N C_N)^2}$ $\frac{dC_{CHB}}{d\tau}=\frac{\rho\kappa_2 C_{DBT}}{(1+K_N C_N)^2}$ $\frac{dC_N}{d\tau}=\frac{-\rho\kappa_3 C_N}{(1+K_N C_N)^2}$ $\frac{dC_{NN}}{d\tau}=\frac{\rho\kappa_3 C_N}{(1+K_N C_N)^2}$	$E_1 = 28.3 \pm 26.8$ $\ln \kappa_{0,1} = 9.5 \pm 5.4$ $T_{ref,1} = 562$ $E_2 = 160.7 \pm 28.6$ $\ln \kappa_{0,2} = 33.8 \pm 5.7$ $T_{ref,2} = 583$ $E_3 = 98.1 \pm 26.6$ $\ln \kappa_{0,3} = 23.4 \pm 5.3$ $T_{ref,3} = 579$ $\Delta H_{ads,N} = -74.8 \pm 28.9$ $\ln K_{N,0} = -11.5 \pm 5.9$ $T_{ref,4} = 553$	$\chi^2_{min} = 75.9$ $\chi^2_{max} = 131.8$ $F_{obj} = 107.3$ $n_p = 8$ $AIC_c = 17.7$	$E_1 = 20.1 \pm 8.0$ $\ln \kappa_{0,1} = 7.5 \pm 1.6$ $T_{ref,1} = 579$ $E_2 = 255.0 \pm 8.6$ $\ln \kappa_{0,2} = 52.8 \pm 1.7$ $T_{ref,2} = 603$ $E_3 = 170.5 \pm 17.5$ $\ln \kappa_{0,3} = 38.0 \pm 3.6$ $T_{ref,3} = 584$ $\Delta H_{ads,N} = -121.0 \pm 26.5$ $\ln K_{N,0} = -23.6 \pm 6.2$ $T_{ref,4} = 553$	$\chi^2_{min} = 75.9$ $\chi^2_{max} = 131.8$ $F_{obj} = 1144.1$ $n_p = 8$ $AIC_c = 13.0$
LPI*	$\frac{dC_{DBT}}{d\tau}=-\rho k_1 C_{DBT}$ $\frac{dC_{BP}}{d\tau}=\rho k_1 C_{DBT}$ $\frac{dC_N}{d\tau}=-\rho k_2 C_N$ $\frac{dC_{NN}}{d\tau}=\rho k_2 C_N$	$E_1 = 98.3 \pm 11.8$ $\ln k_{0,1} = 23.1 \pm 2.4$ $T_{ref,1} = 562$ $E_2 = 467.9 \pm 84.8$ $\ln k_{0,2} = 98.4 \pm 17.5$ $T_{ref,2} = 579$	$\chi^2_{min} = 60.5$ $\chi^2_{max} = 111.2$ $F_{obj} = 165.5$ $n_p = 4$ $AIC_c = 0.1$	$E_1 = 77.4 \pm 5.1$ $\ln k_{0,1} = 19.5 \pm 1.1$ $T_{ref,1} = 579$ $E_2 = 173.8 \pm 13.9$ $\ln k_{0,2} = 38.6 \pm 2.9$ $T_{ref,2} = 584$	$\chi^2_{min} = 60.5$ $\chi^2_{max} = 111.2$ $F_{obj} = 455.5$ $n_p = 4$ $AIC_c = -1.9$

Table 3. Estimated parameters and statistics for simultaneous DBT HDS and Q HDN on CoMoP and NiMoP catalysts with different modeling approaches (cont.)

Model	Equation	CoMoP		NiMoP	
		Parameter	Statistical metrics	Parameter	Statistical metrics
LHI*	$\frac{dC_{DBT}}{dt}=\frac{-\rho\kappa_1 C_{DBT}}{(1+K_N C_N)^2}$ $\frac{dC_{BF}}{dt}=\frac{\rho\kappa_1 C_{DBT}}{(1+K_N C_N)^2}$ $\frac{dC_N}{dt}=\frac{-\rho\kappa_2 C_N}{(1+K_N C_N)^2}$ $\frac{dC_{NN}}{dt}=\frac{\rho\kappa_2 C_N}{(1+K_N C_N)^2}$	E_1=43.9 ±26.1 $\ln \kappa_{0,1}$ =12.7 ±5.3 E_2=105.9 ± 26.1 $\ln \kappa_{0,2}$ =24.9 ± 5.3 $\Delta H_{ads,N}$=65.4 ± 31.3 $\ln K_{N,0}$ =9.7 ±6.4	χ^2_{min} = 58.8 χ^2_{max} = 108.9 F_{obj}=66.5 n_p=6 AIC=3.6 AIC_c=9.2	E_1=77.6 ± 10.6 $\ln \kappa_{0,1}$ =19.6 ± 2.2 E_2=167.9 ± 15.2 $\ln \kappa_{0,2}$ =37.4 ± 3.1 $\Delta H_{ads,N}$=18.3 ± 184.8 $\ln K_{N,0}$ =5.0 ± 38.2	χ^2_{min} = 58.8 χ^2_{max} = 108.9 F_{obj}=451.6 n_p=6 AIC= -0.2 AIC_c= 5.4
LPIH	$\frac{dC_{DBT}}{d\tau}=-\rho k_1 C_{DBT}-\rho k_2 C_{DBT} C_{H2}$ $\frac{dC_{BP}}{d\tau}=\rho k_1 C_{DBT}$ $\frac{dC_{CHB}}{d\tau}=\rho k_2 C_{DBT} C_{H2}$ $\frac{dC_N}{d\tau}=-\rho k_3 C_N$ $\frac{dC_{NN}}{d\tau}=\rho k_3 C_N$	E_1=92.4 ±11.8 $\ln k_{0,1}$ =21.9 ±2.4 $T_{ref,1}$=562 E_2=247.4 ±23.1 $\ln k_{0,2}$ =51.6 ±4.6 $T_{ref,2}$=583 E_3=468.1 ±84.8 $\ln k_{0,3}$ =98.5 ±17.5 $T_{ref,3}$=579	χ^2_{min} = 77.7 χ^2_{max} = 134.1 F_{obj}=241.5 n_p=6 AIC_c=6.6	E_1=50.5 ± 3.9 $\ln k_{0,1}$ =13.6 ±0.8 $T_{ref,1}$=579 E_2=265.4 ± 7.0 $\ln k_{0,2}$ =55.7 ±1.4 $T_{ref,2}$=603 E_3=173.8 ±13.9 $\ln k_{0,3}$ =38.5 ±2.9 $T_{ref,3}$=584	χ^2_{min} = 77.7 χ^2_{max} = 134.1 F_{obj}=1219.9 n_p=6 AIC_c=3.4

As the κ_i constants of the LH models are the result of the product of several constants, it can be difficult to compare different LH models. When comparing the LPG and LPI models, it can be noticed that for HDS, the global apparent activation energy (E_1 in LPG) is found between the apparent activation energies of each of the reaction routes (E_1 and E_2 in LPI), where $E_2 > E_1$. Furthermore, it can be noticed that the "global" apparent energy value is closer to the DDS than HYD route, mainly for CoMoP. This reflects the fact that the preferential route of HDS is DDS for both catalysts, especially CoMoP.

When evaluating the same models between the two catalysts, it can be noticed that CoMoP presents higher apparent activation energies in the "global" route of HDS and HDN, while NiMoP presents higher apparent activation energies in the HYD route of HDS. This observation was attributed to the fact that the nickel catalyst can promote the hydrogenation steps of the HDN reaction more easily. Thus, due to the high adsorption constants, the nitrogen-containing species do not contain enough energy to desorb, and the HYD route of HDS is disadvantaged and increases the activation energy of such route.

The Akaike Information Criterion Corrected (AIC_c) is a statistical metric used to compare models of a different number of parameters [85]. It assumes that the model errors are normally and independently distributed and normalizes the objective function obtained in the estimation by the number of degrees of freedom in the system (considering the number of parameters and data points). The AIC_c values were calculated for each tested model (Table 3). The obtained AIC_c values suggest that Model LHI was the best for catalyst CoMoP (AIC_c 17.7) and NiMoP (AIC_c13.0). Considering PL models, models with individual HDS reactions are the best models by the criterion of Akaike for the cobalt catalyst (AIC_c6.8) and the nickel catalyst (AIC_c3.4). Correlation coefficients between the experimental and predicted concentrations of each compound by the LPI and LHI models are described in Table 4.

Table 4. Correlation coefficients for LPI and LHI models for each catalyst.

Model	Compound	Catalyst	
		CoMoP	NiMoP
LPI	DBT	0.98	0.94
	BP	0.98	0.89
	CHB	0.98	0.99
	N	0.99	1.00
	NN	0.95	0.99
LHI	DBT	0.98	0.92
	BP	0.98	0.84
	CHB	0.98	0.99
	N	1.00	1.00
	NN	0.98	0.99

LPI for CoMoP and NiMoP and LHI for NiMoP models resulted in final objective function values that were above the maximum chi-square value. This indicates that the models were not able to explain the experimental errors, as the average calculated prediction errors were larger than the experimental ones (although, in principle, the experimental errors might have also been underestimated). In general, PL models also resulted in final objective function values above the upper limit of the chi-square distribution, indicating that these models were not able to explain the experimental deviations satisfactorily [86]. On the other hand, the correlation coefficients between the experimental and model-predicted concentrations of each evaluated compound were always larger than 0.9, suggesting that the models presented satisfactory performances, despite not describing the available experimental data within the experimental precision, possibly because of the simple proposed kinetic schemes (Table 4). For this reason, activation energy and pre-exponential factor values were statistically significant and the parametric correlation matrix did not display strong correlations between

pairs of model parameters (below 0.7), making the parameter estimates statistically satisfactory, since the obtained estimates were essentially independent of each other [86]. Experimental data (Section S1 – Tables S1 to S4) and variances (Section S2 – Table S5), statistical estimation analyses and data-to-model graphs of all evaluated models (LPG, LPI, LHG, LHI, LPI*, LHI* and LPIH) (Section S3 – Tables S6 to S28 and Figures S1 to S12) can be found in Supplementary Information.

3.4. Statistical Interpretation of the LHI Model

A more detailed investigation of the parametric correlation matrix of the best model (LHI) for the CoMoP and NiMoP catalysts (Tables 5 and 6, respectively) highlights that, for CoMoP, there was a moderate correlation (above 0.7) between the pairs b_1-a_4, b_1-b_4 and a_4-b_4 and a strong correlation between the pair a_2-b_2 (above 0.9). In the NiMoP case, there was a moderate correlation between a_4-b_4 and a strong correlation between a_3-b_3. These findings result from the inherent mathematical structure of the proposed model and encourages the use of reparametrization schemes. It is worth mentioning that alternative reparametrization strategies of LH model equations that decorrelate the estimated parameters are necessary and constitutes a gap in the scientific literature.

Table 5. Parametric correlation matrix for the LHI CoMoP model.

	a_1	b_1	a_2	b_2	a_3	b_3	a_4	b_4
a_1	1.00E+00	-1.15E-02	2.42E-01	4.07E-02	3.83E-01	4.27E-01	2.97E-01	-1.64E-01
b_1	-1.15E-02	1.00E+00	5.58E-01	6.62E-01	7.30E-02	5.10E-01	8.72E-01	7.99E-01
a_2	2.42E-01	5.58E-01	1.00E+00	9.68E-01	2.15E-01	4.26E-01	5.90E-01	3.67E-01
b_2	4.07E-02	6.62E-01	9.68E-01	1.00E+00	1.37E-01	3.79E-01	6.20E-01	4.98E-01
a_3	3.83E-01	7.30E-02	2.15E-01	1.37E-01	1.00E+00	-1.99E-01	1.43E-01	-2.14E-01
b_3	4.27E-01	5.10E-01	4.26E-01	3.79E-01	-1.99E-01	1.00E+00	6.73E-01	3.81E-01
a_4	2.97E-01	8.72E-01	5.90E-01	6.20E-01	1.43E-01	6.73E-01	1.00E+00	8.14E-01
b_4	-1.64E-01	7.99E-01	3.67E-01	4.98E-01	-2.14E-01	3.81E-01	8.14E-01	1.00E+00

Table 6. Parametric correlation matrix for the LHI NiMoP model.

	a_1	b_1	a_2	b_2	a_3	b_3	a_4	b_4
a_1	1.00E+00	4.71E-02	6.72E-01	1.13E-01	4.10E-01	2.66E-01	5.71E-01	-5.91E-01
b_1	4.71E-02	1.00E+00	-6.31E-01	6.47E-01	3.68E-01	2.43E-01	6.77E-01	-2.13E-01
a_2	6.72E-01	-6.31E-01	1.00E+00	-5.14E-01	4.37E-02	2.86E-02	-5.52E-02	-2.66E-01
b_2	1.13E-01	6.47E-01	-5.14E-01	1.00E+00	3.48E-01	2.26E-01	5.79E-01	-3.35E-01
a_3	4.10E-01	3.68E-01	4.37E-02	3.48E-01	1.00E+00	9.51E-01	6.55E-01	-5.96E-01
b_3	2.66E-01	2.43E-01	2.86E-02	2.26E-01	9.51E-01	1.00E+00	4.27E-01	-3.79E-01
a_4	5.71E-01	6.77E-01	-5.52E-02	5.79E-01	6.55E-01	4.27E-01	1.00E+00	-7.72E-01
b_4	-5.91E-01	-2.13E-01	-2.66E-01	-3.35E-01	-5.96E-01	-3.79E-01	-7.72E-01	1.00E+00

Figures 5 and 6 show the experimental concentrations and respective values predicted by the LHI model for CoMoP and NiMoP, respectively.

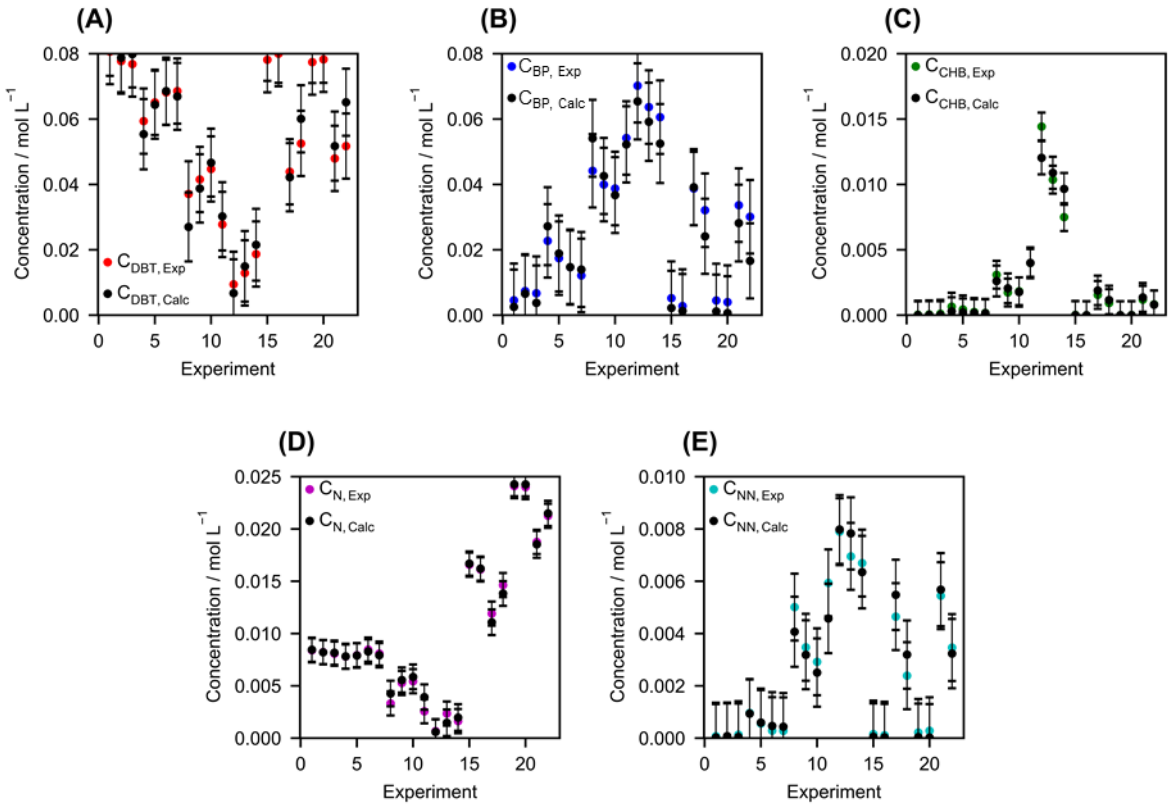

Figure 5. Concentrations predicted by the LHI model and observed experimentally – CoMoP.

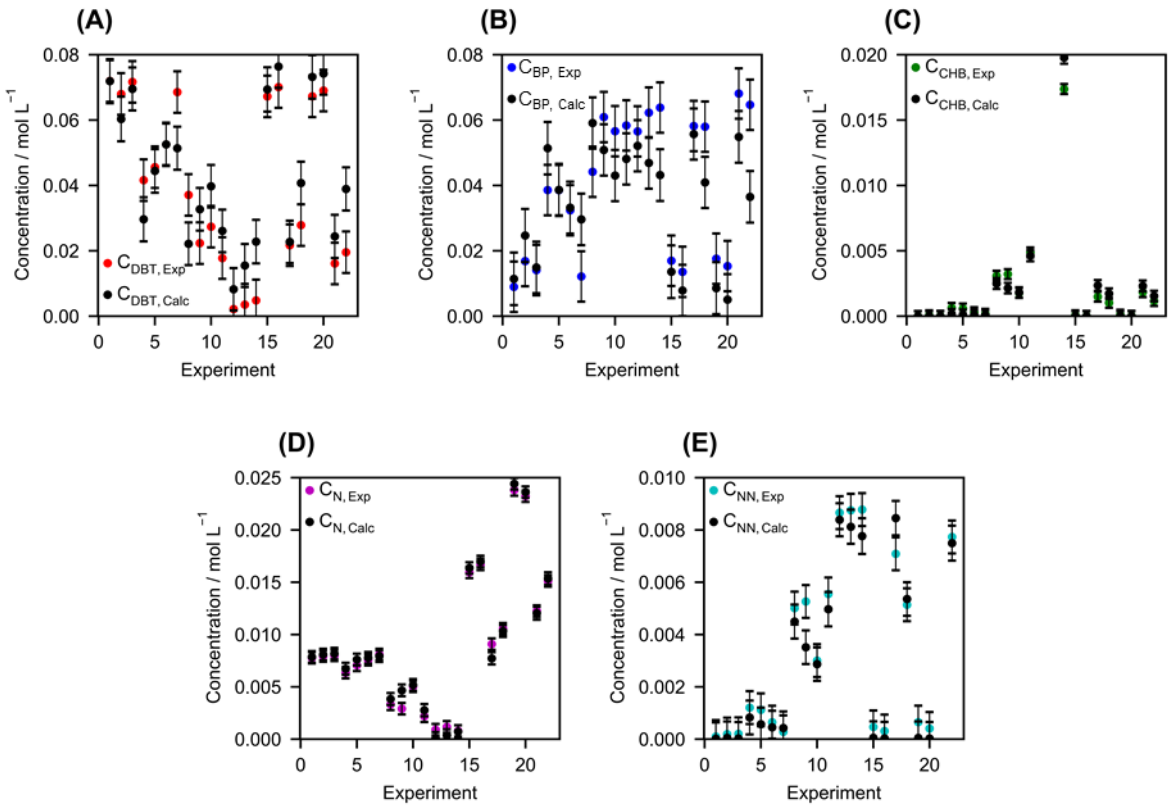

Figure 6. Concentrations predicted by the LHI model and observed experimentally – NiMoP.

With the mathematical structure of the model and the estimated parameter values, simulation curves of concentrations calculated as functions of the spatial time were built for temperatures of 250 °C and 280 °C for feed containing 150 mg.kg^{-1} of initial N for both catalysts. The experimental points selected for validation, 250 °C, 22 h^{-1} and 150 mg.kg^{-1} and 280 °C, 16 h^{-1} and 150 °C, were plotted on the curve, taking into account the experimental error. Figure 7 illustrates the validation of the LHI model.

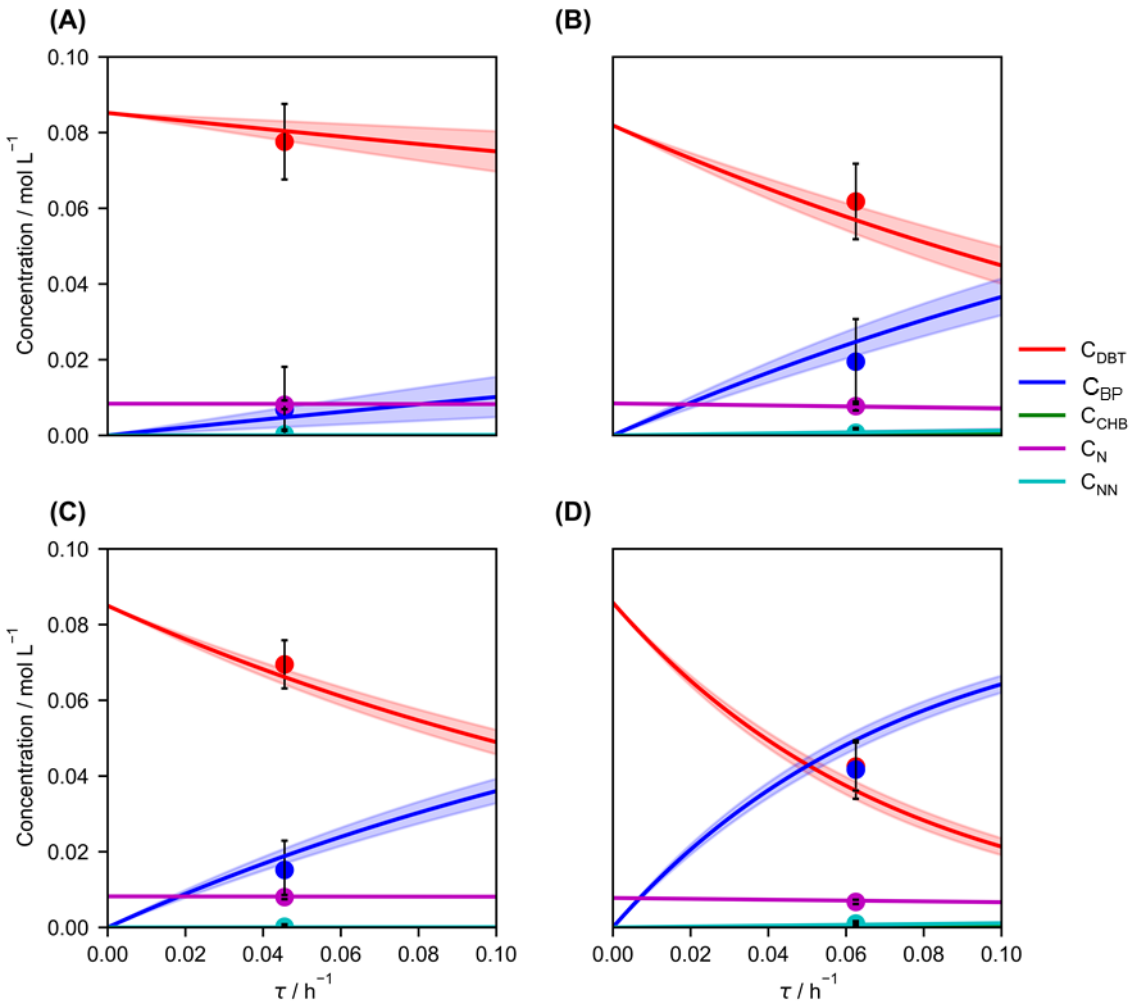

Figure 7. Validation of the LHI model for CoMoP (A and B) and NiMoP (C and D) for two different operation conditions at 150 mg.kg^{-1} N. Condition 1: 250 °C, 22 h^{-1} and condition 2: 280 °C, 16 h^{-1}.

In this perspective, the LHI model can be admitted as valid in the evaluated experimental region, as it satisfactorily predicted the obtained results when considering the prediction and experimental errors. The larger prediction error for CoMoP (Figures 7 (A) and (B)) was expected, given the higher values of the parametric errors obtained during the estimation in this case. Furthermore, this can also be due to the larger parametric correlation when compared to the NiMoP model parameters (Figures 7 (C) and (D)).

The estimation of two new parameters, when considering the CHB formation route in the kinetic modeling, may be difficult because the experimental concentrations of CHB were

mostly lower than 0.015 mol.L^{-1}. Therefore, the information (input variables) inserted in the system to infer these parameters is close to zero. Individual models disregarding the formation of CHB, LPI* (Power Law Individual without CHB) and LHI* (Langmuir Hinshelwood without CHB). The estimation results are shown in Table 3.

As expected, the obtained CoMoP catalyst model did not provide statistically different mdomodel outputs. This fact was related to the low concentrations of CHB obtained experimentally for the cobalt catalyst, bringing little information as an input variable in the system. However, some differences could be observed for the nickel catalyst since, under some conditions, CHB reached concentrations close to 0.020 mol.L^{-1}.

The last investigated model (LPIH) was evaluated by Nascimento et al. (2021) [64] after the addition of quinoline to the feed. This model is analogous to model LPI but considers order 1 with respect to the concentration of dissolved hydrogen in the liquid phase. The same catalysts, feed, and reaction unit were used in the present work. The model assumes order one with respect to hydrogen in the HDS HYD route. The result of the model estimation is shown in Table 3. The effect of hydrogen concentration on the modeling of the CHB formation route resulted in statistically similar model parameters when comparing the LPI and LPIH models for both catalysts. In general, the presence of quinoline did not affect the estimated values for the apparent activation energy, when considering the global model (102 ± 13 kJ.mol^{-1} (CoMoP) and 94 ± 8 kJ.mol^{-1} (NiMoP), as proposed by Nascimento et al. (2021) [64], and 109 ± 18 kJ.mol^{-1} (CoMoP) and 84 ± 7 kJ.mol^{-1} (NiMoP) in the present work). For the apparent activation energy of the DDS route, results were also statistically equivalent (100 ± 10 kJ.mol^{-1} (CoMoP) and 90 ± 7 kJ.mol^{-1} (NiMoP), as proposed by Nascimento et al. (2021) [64], and 92 ± 12 kJ.mol^{-1} (CoMoP) and 50 ± 4 kJ.mol^{-1} (NiMoP) in the present work). However, in the HYD route, there was a significant increase of the estimated activation energy (101 ± 13 kJ.mol^{-1} (CoMoP) and 95 ± 8 kJ.mol^{-1} (NiMoP) in Nascimento et al. (2021) [64],

compared to 230 ± 23 kJ.mol^{-1} (CoMoP) and 275 ± 7 kJ.mol^{-1} (NiMoP) in the present work), mainly for the nickel catalyst, reinforcing that the nitrogenous species are adsorbed in the HYD sites, making more difficult the formation of CHB through the HYD route of the HDS.

Although it is not easy to compare kinetic parameters reported in the literature, given differences in reactor configurations, reaction conditions, loads, and catalysts of different compositions, we sought to compare the inferred activation energy and adsorption enthalpy values at conditions similar to those used in the present work. For HDS of DBT, it could be noticed that the apparent activation energy values found in the global model were consistent with those reported by Farag et al. (2000) [27] when studying the HDS kinetics of DBT using a CoMoP/Al_2O_3 catalyst (146.4 kJ.mol^{-1}) and by Feng et al. (2018) [78] when evaluating the same reaction in a catalyst promoted by nickel (94.97 kJ.mol^{-1}). However, when evaluating the individual models (LPI), it was noticed that the apparent activation energy for CHB formation was higher in the present work than the ones reported by Chen et al. (2010) [88] using a cobalt catalyst (92 kJ.mol^{-1}).

Some reports did not use nitrogen-containing molecules simultaneously with DBT, which could explain some of the observed differences. Apparent activation energy data for HDN reactions using a CoMoP bed were not found in the literature. However, the values found by Girgis and Gates (1991) [10] for a NiMo bed were of the same order of magnitude of the ones obtained in the present work. It is worth mentioning that the global model used for HDN reactions considers adsorption and inhibition effects coupled to kinetics in k_{HDN} values, so that the obtained apparent activation energy was actually a sum of the contributions of the activation energies for the reaction and the adsorption enthalpies of the most adsorbed intermediates at the catalyst sites.

The LHI model predicted statistically significant values for the adsorption enthalpies of nitrogen for both catalysts. Miller and Hineman (1984) [57] estimated the enthalpy of

adsorption for quinoline HDN and found the value of -112 kJ.mol^{-1}. In the present work, the adsorption enthalpy of nitrogen-containing species was equal to -74.8 ± 28.9 kJ.mol^{-1} and -121.0 ± 26.5 kJ.mol^{-1}, as estimated for the cobalt and nickel catalysts, respectively. Laredo et al. (2003) [89] reported the adsorption constant of indole and o-ethylaniline in the presence of DBT (675 mg.kg^{-1} S, 320 °C, and 5.1 MPa). The reported values were equal to 349.2 and 34.1 L.mol^{-1}, respectively. The LHI yields an adsorption constant of nitrogen-containing species of 38.7 L.mol^{-1} under similar conditions, which agrees with the observation made by Laredo et al. (2001) [90] that the nitrogen-containing intermediates cover the active sites and are the most difficult to desorb.

In another effort to compare the catalytic activity of the materials used in this work with others reported in the literature, the turnover frequency (TOF) values were calculated for different experimental conditions: condition 1 (250 °C, 28 h^{-1}, 150 mg.kg^{-1} N), condition 2 (250 °C, 28 h^{-1}, 450 mg.kg^{-1} N), condition 3 (310 °C, 16 h^{-1}, 150 mg.kg^{-1} N), and condition 4 (310 °C, 16 h^{-1}, 450 mg.kg^{-1} N). The LHI model exhibited both physical and statistical significance when compared to the others and was selected for rate calculations.

The analysis starts by determining the MoS_2 concentration in both catalysts, based on the XPS atomic concentration assigned to [Mo^{4+}] (Eq. 10) and the mass of molybdenum in the materials (C(Mo)), to evaluate the C_{MoS_2} effective concentration (% w/w) (Eq. 11):

$$[Mo^{4+}] = \frac{A_{\mathrm{Mo^{4+}/Al}}}{A_{\mathrm{Mo^{4+}/Al}} + A_{\mathrm{Mo^{4+}/Al}} + A_{\mathrm{Mo^{4+}/Al}}} \tag{10}$$

where A_i is the atomic concentration of species i, as described by the XPS.

$$C_{MoS_2} = [Mo^{4+}] \times C(Mo) \tag{11}$$

TOF values were then calculated according to Eq. 12 by dividing the normalized initial reaction rate ($_j$) provided by the LHImodel at the specified condition by the number of active sites available in the catalysts, as described by Eq. 12 and presented in Table 7.

$$\mathrm{TOF}_j = \frac{(r_j)\, MM_{Mo}}{C_{MoS_2}\, D} \tag{12}$$

where j represents the DDS, HYD and HDN reaction routes, $MM_{Mo}$is the molar mass of molybdenum (95.95 g mol^{-1}), and D is the degree of dispersion of Mo species, obtained by HRTEM.

Table 7. TOF values for CoMoP and NiMoP catalysts for HDS and HDN reactions routes at different reaction conditions using model LHI.

	CoMoP			NiMoP		
	TOF_{DDS} (h^{-1})	TOF_{HYD} (h^{-1})	TOF_{HDN} (h^{-1})	TOF_{DDS} (h^{-1})	TOF_{HYD} (h^{-1})	TOF_{HDN} (h^{-1})
Cond. 1	0.6	0.0013	0.007	4.8	0.0008	0.008
Cond. 2	0.1	0.0002	0.003	1.6	0.0003	0.008
Cond. 3	6.6	0.3	0.4	17.4	0.7	1.0
Cond. 4	2.7	0.1	0.5	15.8	0.7	2.7

Condition 1 (250 °C, 28 h^{-1}, 150 mg.kg^{-1} N); Condition 2 (250 °C, 28 h^{-1}, 450 mg.kg^{-1} N); Condition 3 (310 °C, 16 h^{-1}, 150 mg.kg^{-1} N), and Condition 4 (310 °C, 16 h^{-1}, 450 mg.kg^{-1} N).

One must note that the increase of the initial quinoline concentration under low conversion conditions (1 and 2) causes a reduction in TOF values for both catalysts, being the HDS the most affected, with a decrease of about 83 % for CoMoP and 66% for NiMoP. TOF_{HDN} values dropped about 57 % for CoMoP catalyst and stayed the same for catalyst NiMoP. At high conversion conditions (3 and 4), the increase of the initial quinoline concentration led to a decrease in TOF_{HDS} values of about 60 % for CoMoP and 10 % for NiMoP catalyst. TOF_{HDN} increased for both catalysts, being more significant for the material

promoted with nickel. The TOF_{HYD} values at high conversions stayed the same for NiMoP. The results can be rationalized in the following matter: at 250 ºC, K_N the adsorption of nitrogen-containing species is much higher than at 310 ºC, which causes both HDS and HDN reactions to be inhibited by such adsorption. When the temperature rises, the sites become more available for the reaction and even the HDN reaction occurs more often. The fact that the TOF_{HYD} values are slightly reduced compared to TOF_{DDS} ones supports the hypothesis that CHB (the HDS hydrogenation product) and HDN compete for active sites of similar nature. Moreover, one must note that TOF values are bigger for the catalyst promoted by nickel compared to those obtained for the material promoted by cobalt. This result agrees with the degree of promotion values in XPS data, which suggests the formation of active sites of enhanced activity (type II).

Lu et al. (2007) [91] reported 46.8 h^{-1} for HDN of quinoline at 340 ºC using a NiMo catalyst. In the present work, a TOF_{HDN} value of 5.9 h^{-1} was found at the same temperature, highlighting the differences related to catalyst composition and kinetic models. A similar trend was observed when comparing the data reported by Braggio et al. (2019) [92] for DBT HDS in the presence of quinoline. The authors reported TOF_{HDS} value of 0.53 h^{-1} and TOF_{HDN} value of 0.13 h^{-1} at 245 ºC for a NiMo catalyst prepared with citric acid and containing 120 $mg.kg^{-1}$ N in the feed. The data obtained here at similar conditions but with 150 $mg.kg^{-1}$ N resulted in values of 3.6 h^{-1} for TOF_{HDS} and 0.004 h^{-1} for TOF_{HDN}. The discrepancies observed in TOF values can be attributed to the fact that TOF values are highly dependent on catalyst composition, the way reaction rates are determined and how the active sites are dosed.

The competitive and inhibition effects resulting from the presence of quinoline in the feed were also analyzed by comparing the data obtained here with those previously by Nascimento et al. (2021) [64] using the same catalysts but with a feed containing DBT only. TOF_{HDS} values were calculated at 270 ºC, 60 bar, and 8 h^{-1} for both catalysts in the presence

and absence of quinoline (Table 8). One can observe the decrease of the HDS rate constant for both catalysts when quinoline was added because of the competition for the active sites. TOF_{HDS} values follow the same trend, according to the competition and inhibition caused by the presence of nitrogen-containing species in the feedstock.

Table 8. TOF values for CoMoP and NiMoP catalysts at 270 ºC and 8 h^{-1} using the LPG model.

	CoMoP			NiMoP		
	k_{HDS}	$TOF_{HDS,0}$	$TOF_{HDN,0}$	k_{HDS}	$TOF_{HDS,0}$	$TOF_{HDN,0}$
Nascimento *et al.*	24.1	8.5	-	20.1	13.1	-
This work	8.3	2.9	0.0002	9.3	6.0	0.1

$C_{DBT,0}$ [=] C_{DBT} [=] mmol L^{-1}; k_{HDS} [=] L h^{-1} kg^{-1}; $TOF_{HDS,0}$ [=] TOF_{HDS} [=] h^{-1}

4. Conclusions

The kinetic study performed for the simultaneous reactions of DBT HDS and quinoline HDN showed that the quinoline HDN and the HDS HYD pathway occur at the hydrogenation sites of the evaluated catalysts. Furthermore, it was shown that the catalyst promoted by nickel presented higher hydrogenating power than cobalt.

The statistical analyses indicated that the kinetic parameters estimated for Langmuir-Hinshelwood models could be strongly correlated due to the intrinsic mathematical structure of these models, even after reparameterization and optimization of reference temperatures. Despite that, the model parameters yielded good fits in terms of the correlation coefficient between experimental and calculated data and according to independent data validation.

Finally, TOF values were calculated, highlighting how adsorption and competition between nitrogen-containing compounds and sulfur-containing compounds can affect reaction pathways. The proposed analyses showed that a catalyst with more hydrogenating power is also more capable of performing both HDN and HDS reactions simultaneously.

Credit authorship contribution statement

M.A.P.S and M.D.M conceived and directed the work. G.S.G.J. obtained the experimental reaction data and did all the parameter estimation with their statistical analysis. I.G.N synthesized the materials and obtained some of the experimental reaction data. M.A. and J.A.B. obtained the XPS data. C.K. and J.T. obtained the HRTEM data. J.C.P. helped with statistical analysis of the data. The manuscript was written mainly by G.S.G.J and M.D.M. with contributions by M.A.P.S., and with input from all authors. All authors have approved the final version of the manuscript.

Declaration of Competing Interest

The authors declare that they have no known competing financial interests or personal relationships that could have appeared to influence the work reported in this paper.

Data availability

Data will be made available on request.

Acknowledgements

Gentil de Souza Guedes Junior acknowledge CAPES for their financial support.

Appendix A. Supplementary data

Supplementary data to this article can be found online at

References

[1] Absi-Halabi M, Stanislaus A, Qabazard H. Trends in catalysis research to meet future refining needs. Hydrocarb Process 1997;2:45–55.

[2] Xiao Z, Li Q, Wang W, Li G, Lin G, Li X, et al. Effects of temperature and time on the facile low-temperature pre-sulfurization of tube-like unsupported Co-Mo catalysts for hydrodesulfurization. Mol Catal 2022;528:112470. https://doi.org/10.1016/j.mcat.2022.112470.

[3] Castillo-Villalón P, Ramírez J, Reyes-Sosa A, Gutiérrez-Alejandre A, Leyva-Ramírez E, Cuevas R, et al. On the contribution of the cobalt sulfide phase to the global activity of industrial-type CoMo/Al2O3 catalysts in the HDS of DBT. Catal Today 2022;394–396:41–9. https://doi.org/10.1016/j.cattod.2021.11.001.

[4] Scherzer J, Gruia A. Hydrocracking Science and Technology. New York: CRC Press; 1996.

[5] Kressmann S, Morel F, Harlé V, Kasztelan S. Recent developments in fixed-bed catalytic residue upgrading. Catal Today 1998;43:203–15.

[6] Sun M, Nicosia D, Prins R. The effects of fluorine, phosphate and chelating agents on hydrotreating catalysts and catalysis. Catal Today 2003;86:173–89.

[7] Lauritsen J V., Olesen GH, Moses PG, Hinnemann B, Helveg S, Nørskov JK, et al. Location and coordination of promoter atoms in Co- and Ni-promoted MoS2-based hydrotreating catalysts. J Catal 2007;249:220–33.

[8] Breysse M, Djega-Mariadassou G, Pessayre S, Geantet C, Vrinat M, Pérot G, et al. Deep desulfurization: reactions, catalysts and technological challenges. Catal Today 2003;84:129–38.

[9] Knudsen KG, Cooper BH, Topsøe H. Catalyst and process technologies for ultra low sulfur diesel. Appl Catal A Gen 1999;189:205–15.

[10] Girgis MJ, Gates BC. Reactivities, reaction networks, and kinetics in high-pressure catalytic hydroprocessing. Ind Eng Chem Res 1991;30:2021–58.

[11] Stanislaus A, Marafi A, Rana MS. Recent advances in the science and technology of ultra low sulfur diesel (ULSD) production. Catal Today 2010;153:1–68.

[12] Sundaramurthy V, Dalai AK, Adjaye J. The effect of phosphorus on hydrotreating property of NiMo/γ-Al2O3 nitride catalyst. Appl Catal A Gen 2008;335:204–10.

[13] Villarroel M, Baeza P, Gracia F, Escalona N, Avila P, Gil-Llambías FJ. Phosphorus effect on Co//Mo and Ni//Mo synergism in hydrodesulphurization catalysts. Appl Catal A Gen 2009;364:75–9.

[14] Usman, Yamamoto T, Kubota T, Okamoto Y. Effect of phosphorus addition on the active sites of a Co-Mo/Al2O3 catalyst for the hydrodesulfurization of thiophene. Appl Catal A Gen 2007;328:219–25.

[15] Dorneles De Mello M, De Almeida Braggio F, Da Costa Magalhães B, Zotin JL, Da Silva MAP. Effects of Phosphorus Content on Simultaneous Ultradeep HDS and HDN Reactions over NiMoP/Alumina Catalysts. Ind Eng Chem Res 2017;56:10287–99. https://doi.org/10.1021/acs.iecr.7b02718.

[16] Macaud M, Milenkovic A, Schulz E, Lemaire M, Vrinat M. Hydrodesulfurization of alkyldibenzothiophenes: evidence of highly unreactive aromatic sulfur compounds. J Catal 2000;193:255–63.

[17] Whitehurst DD, Isoda T, Mochida I. Present state of the art and future challenges in the hydrodesulfurization of polyaromatic sulfur compounds. Adv Catal 1998;42:345–471.

[18] Houalla M, Nag NK, Broderick DH, Gates BC. Hydrodesulfurization of dibenzothiophene catalyzed by sulfided CoO-MoO3 γ-Al2O3: the reaction network. AlChE J 1978;24:1015–21.

[19] Singhal GH, Espino RL, Sobel JE, Huff GA. Hydrodesulfurization of sulfur heterocyclic compounds: kinetics of dibenzothiophene. J Catal 1981;67:457–68.
[20] Landau M V. Deep hydrotreating of middle distillates from crude and shale oils. Catal Today 1997;36:393–429.
[21] Houalla M, Broderick DH, Sapre A V., Nag NK, de Beer VHJ, Gates BC, et al. Hydrodesulfurization of methyl-substituted dibenzothiophenes catalyzed by sulfided CoMo γ-Al2O3. J Catal 1980;61:523–7.
[22] Singhal GH, Espino RL, Sobel JE. Hydrodesulfurization of sulfur heterocyclic compounds: reaction mechanisms. J Catal 1981;67:446–56.
[23] Meille V, Schulz E, Lemaire M, Vrinat M. Hydrodesulfurization of alkyldibenzothiophenes over a NiMo/Al2O3 catalyst: kinetics and mechanism. J Catal 1997;170:29–36.
[24] Michaud P, Lemberton JL, Pérot G. Hydrodesulfurization of dibenzothiophene and 4,6-dimethyldibenzothiophene: Effect of an acid component on the activity of a sulfided NiMo on alumina catalyst. Appl Catal A Gen 1998;169:343–53.
[25] Bataille F, Lemberton JL, Michaud P, Pérot G, Vrinat M, Lemaire M, et al. Alkyldibenzothiophenes Hydrodesulfurization-Promoter Effect, Reactivity, and Reaction Mechanism. J Catal 2000;191:409–22. https://doi.org/10.1006/jcat.1999.2790.
[26] Orozco EO, Vrinat M. Kinetics of dibenzothiophene hydrodesulfurization over MoS2 supported catalysts: modelization of the H2S partial pressure effect. Appl Catal A Gen 1998;170:195–206.
[27] Farag H, Mochida I, Sakanishi K. Fundamental comparison studies on hydrodesulfurization of dibenzothiophenes over CoMo-based carbon and alumina catalysts. Appl Catal A Gen 2000;194:147–57.
[28] Laine RM. Comments on the mechanisms of heterogeneous catalysis of the hydrodenitrogenation reaction. Catal Rev 1983;25:459–74.
[29] Xie D, Liu X, Lv H, Guo Y. Products, pathways, and kinetics for catalytic hydrodenitrogenation of quinoline in hydrothermal condition. J Supercrit Fluids 2022;182:105509. https://doi.org/10.1016/j.supflu.2021.105509.
[30] Jian M, Prins R. Mechanism of the hydrodenitrogenation of quinoline over NiMo(P)/Al2O3 catalysts. J Catal 1998;179:18–27.
[31] Oelderik JM, Sie ST, Bode D. Progress in the catalysis of the upgrading of petroleum residue. A review of 25 Years of R&D on Shell's residue hydroconversion technology. Appl Catal 1989;47:1–24.
[32] Furimsky E. Selection of catalysts and reactors for hydroprocessing. Appl Catal A Gen 1998;171:177–206.
[33] Sadare OO, Daramola MO. Adsorptive desulfurization of dibenzothiophene (DBT) in model petroleum distillate using functionalized carbon nanotubes. Environ Sci Pollut Res 2019;26:32746–58.
[34] Schulz H, Rahman NM. Elementary steps of hydrogenative sulfur-, nitrogen- and oxygen- removal from organic compounds on sulfided catalysts. Stud Surf Sci Catal 1993;75:585–96.
[35] Startsev AN. The mechanism of HDS catalysis. Catal Rev 1995;37:353–422.
[36] Ho TC. Hydrodenitrogenation Catalysis. Catal Rev 1988;30:117–60.
[37] Perot G. The reactions involved in hydrodenitrogenation. Catal Today 1991;10:447–72.
[38] Moreau C, Geneste P. Factors affecting the reactivity of organic model compounds in hydrotreating reactions. Theor. Asp. Heterog. Catal., 1990, p. 256–310. https://doi.org/10.1007/978-94-010-9882-3_7.
[39] Schulz H, Schon M, Rahman NM. Hydrogenative denitrogenation of model compounds

as related to the refining of liquid fuels. vol. 27. Elsevier; 1986.
[40] Ferdous D, Dalai AK, Adjaye J. Hydrodenitrogenation and hydrodesulphurization of heavy gas oil using NiMo/Al2O3 catalyst containing phosphorus: experimental and kinetic studies. Can J Chem Eng 2005;83:855–64.
[41] Rodríguez MA, Ancheyta J. Modeling of hydrodesulfurization (HDS), hydrodenitrogenation (HDN), and the hydrogenation of aromatics (HDA) in a vacuum gas oil hydrotreater. Energy and Fuels 2004;18:789–94.
[42] Jiménez F, Kafarov V, Nuñez M. Modeling of industrial reactor for hydrotreating of vacuum gas oils. Simultaneous hydrodesulfurization, hydrodenitrogenation and hydrodearomatization reactions. Chem Eng J 2007;134:200–8.
[43] Bezergianni S, Kalogianni A, Dimitriadis A. Catalyst evaluation for waste cooking oil hydroprocessing. Fuel 2012;93:638–41.
[44] Morales-Guio CG, Stern L-A, Hu X. Nanostructured hydrotreating catalysts for electrochemical hydrogen evolution. Chem Soc Rev 2014;43:6555–69.
[45] Cotta RM, Maciel MRW, Maciel Filho R. Kinetic and reactor models for HDS of middle distillates. Comput Chem Eng Suppl 1999:S791–4.
[46] Novaes L da R, Pacheco ME, Salim VMM, Resende NS de. Accelerated deactivation studies of hydrotreating catalysts in pilot unit. Appl Catal A Gen 2017;548:114–21.
[47] Delmon B, Froment GF, Grange P. Hydrotreatment and hydrocracking of oil fractions 1999.
[48] Sánchez-Delgado RA. Breaking C-S bonds with transition metal complexes. A review of molecular approaches to the study of the mechanisms of the hydrodesulfurization reaction. J Mol Catal 1994;86:287–307.
[49] Mochida I, Choi K-H. An overview of hydrodesulfurization and hydrodenitrogenation. J Japan Pet Inst 2004;47:145–63.
[50] Ho TC, Qiao L. Competitive adsorption of nitrogen species in HDS: Kinetic characterization of hydrogenation and hydrogenolysis sites. J Catal 2010;269:291–301.
[51] Ledesma BC, Martínez ML, Gómez Costa MB, Beltramone AR. Indole HDN Using Iridium Nanoparticles Supported on Titanium Nanotubes. Catal Letters 2022. https://doi.org/10.1007/s10562-022-04221-x.
[52] Novaes L da R, Resende NS de, Salim VMM, Secchi AR. Modeling, simulation and kinetic parameter estimation for diesel hydrotreating. Fuel 2017;209:184–93.
[53] Sigurdson S, Dalai AK, Adjaye J. Hydrotreating of light gas oil using carbon nanotube supported NiMoS catalysts: Kinetic modelling. Can J Chem Eng 2011;89:562–75.
[54] Bej SK, Dalai AK, Adjaye J. Comparison of hydrodenitrogenation of basic and nonbasic nitrogen compounds present in oil sands derived heavy gas oil. Energy & Fuels 2001;15:377–83.
[55] Bej SK, Dalai AK, Adjaye J. Kinetics of hydrodesulfurization of heavy gas oil derived from oil-sands bitumen. Pet Sci Technol 2002;20:867–77.
[56] Sonnemans J, van den Berg GH, Mars P. The mechanism of pyridine hydrogenolysis on molybdenum-containing catalysts: II. Hydrogenation of pyridine to piperidine. J Catal 1973;31:220–30.
[57] Miller JT, Hineman MF. Non-first-order hydrodenitrogenation kinetics of quinoline. J Catal 1984;85:117–26.
[58] Satterfield CN, Cocchetto JF. Reaction network and kinetics of the vapor-phase catalytic hydrodenitrogenation of quinoline. Ind Eng Chem Process Des Dev 1981;20:53–62.
[59] Botchwey C, Dalai AK, Adjaye J. Two-stage hydrotreating of Athabasca heavy gas oil with interstage hydrogen sulfide removal: Effect of process conditions and kinetic analyses. Ind Eng Chem Res 2004;43:5854–61.

[60] Aleksandrov P V., Reshetnikov SI, Bukhtiyarova GA, Noskov AS. Deep hydrodesulfurization of gas oils with high sulfur content: Experiment and kinetic modeling. Chem Eng J 2022;446:137059. https://doi.org/10.1016/j.cej.2022.137059.
[61] Chehadeh D, Ma X, Al Bazzaz H. Recent progress in hydrotreating kinetics and modeling of heavy oil and residue: A review. Fuel 2023;334:126404. https://doi.org/10.1016/j.fuel.2022.126404.
[62] Ferdous D, Dalai AK, Adjaye J. Hydrodenitrogenation and hydrodesulfurization of heavy gas oil using NiMo/Al2O3 catalyst containing boron: experimental and kinetic studies. Ind Eng Chem Res 2006;45:544–52.
[63] Cassol GO, Gallon R, Schwaab M, Barbosa-Coutinho E, Júnior JBS, Pinto JC. Statistical evaluation of non-linear parameter estimation procedures for adsorption equilibrium models. Adsorpt Sci Technol 2014;32:257–73.
[64] Nascimento IG, Locatel W de R, Magalhães B da C, Travalloni L, Zotin JL, Silva MAP da. Kinetics of dibenzothiophene hydrodesulfurization reactions using CoMoP/Al2O3 and NiMoP/Al2O3. Catal Today 2021;381:200–8. https://doi.org/10.1016/j.cattod.2020.07.013.
[65] Bard Y. Nonlinear parameter estimation. 1st ed. New York: Academic Press; 1974.
[66] Bates DM, Watts DG. Nonlinear regression analysis and its applications. New York: John Wiley & Sons; 1988.
[67] Biegler LT, Damiano JJ, Blau GE. Nonlinear parameter estimation: a case study comparison. AIChE J 1986;32:29–45.
[68] Katare S, Bhan A, Caruthers JM, Delgass WN, Venkatasubramanian V. A hybrid genetic algorithm for efficient parameter estimation of large kinetic models. Comput Chem Eng 2004;28:2569–81.
[69] Han W, Nie H, Long X, Li M, Yang Q, Li D. Effects of the support Brønsted acidity on the hydrodesulfurization and hydrodenitrogention activity of sulfided NiMo/Al2O3 catalysts. Catal Today 2017;292:58–66.
[70] Kasztelan S, Toulhoat H, Grimblot J, Bonnelle JP. A geometrical model of the active phase of hydrotreating catalysts. Appl Catal 1984;13:127–59. https://doi.org/10.1016/S0166-9834(00)83333-3.
[71] Glotov AP, Vutolkina A V., Vinogradov NA, Pimerzin AA, Vinokurov VA, Pimerzin AA. Enhanced HDS and HYD activity of sulfide Co-PMo catalyst supported on alumina and structured mesoporous silica composite. Catal Today 2021;377:82–91. https://doi.org/10.1016/j.cattod.2020.10.010.
[72] Soave G. Equilibrium constants from a modified Redlich-Kwong equation of state. Chem Eng Sci 1972;27:1197–203. https://doi.org/10.1016/0009-2509(72)80096-4.
[73] Schwaab M, Biscaia EC, Monteiro JL, Pinto JC. Nonlinear parameter estimation through particle swarm optimization. Chem Eng Sci 2008;63:1542–52.
[74] Nelder JA, Mead R. A simplex method for function minimization. Comput J 1965;7:308–13.
[75] Wang Y. Gauss-Newton method. Wiley Interdiscip Rev Comput Stat 2012;4:415–20.
[76] Schwaab M, Lemos LP, Pinto JC. Optimum reference temperature for reparameterization of the Arrhenius equation. Part 2: Problems involving multiple reparameterizations. Chem Eng Sci 2008;63:2895–906.
[77] Bravo-Sanchez M, Romero-Galarza A, Ramírez J, Gutiérrez-Alejandre A, Solís-Casados DA. Quantification of the sulfidation extent of Mo in CoMo HDS catalyst through XPS. Appl Surf Sci 2019;493:587–92.
[78] Escobar J, Barrera MC, Gutiérrez AW, Cortés-Jacome MA, Angeles-Chávez C, Toledo JA, et al. Highly active P-doped sulfided NiMo/alumina HDS catalysts from Mo-blue by

using saccharose as reducing agents precursor. Appl Catal B Environ 2018;237:708–20.
[79] Santolalla-Vargas CE, Santes V, Ortega-Niño C, Hernández-Gordillo A, Sanchez-Minero F, Lartundo-Rojas L, et al. Effect of trimesic acid as chelating agent in sulfided CoMoP/γ-Al2O3 catalyst for hydrodesulfurization of straight-run gas oil. Catal Today 2020;349:244–55.
[80] Vlasova EN, Bukhtiyarova GA, Deliy I V., Aleksandrov P V., Porsin AA, Panafidin MA, et al. The effect of rapeseed oil and carbon monoxide on SRGO hydrotreating over sulfide CoMo/Al2O3 and NiMo/Al2O3 catalysts. Catal Today 2020;357:526–33.
[81] Nadeina KA, Vatutina Y V., Mukhacheva PP, Krestyaninova V, Saiko A V., Bykova ES, et al. Influence of the order of the catalysts in the stacked bed of VGO hydrotreating catalysts. Fuel 2021;306:121672. https://doi.org/10.1016/j.fuel.2021.121672.
[82] Farag H, Kishida M, Al-Megren H. Competitive hydrodesulfurization of dibenzothiophene and hydrodenitrogenation of quinoline over unsupported MoS2 catalyst. Appl Catal A Gen 2014;469:173–82.
[83] Nguyen M-T, Tayakout-Fayolle M, Pirngruber GD, Chainet F, Geantet C. Kinetic modeling of quinoline hydrodenitrogenation over a NiMo(P)/Al2O3 catalyst in a batch reactor. Ind Eng Chem Res 2015;54:9278–88.
[84] García-Martínez JC, Castillo-Araiza CO, Heredia JA de los R, Trejo E, Montesinos A. Kinetics of HDS and of the inhibitory effect of quinoline on HDS of 4,6-DMDBT over a Ni-Mo-P/Al2O3 catalyst: Part I. Chem Eng J 2012;210:53–62.
[85] Cavanaugh JE. Unifying the derivations for the Akaike and corrected Akaike information criteria. Stat Probab Lett 1997;33:201–8. https://doi.org/10.1016/s0167-7152(96)00128-9.
[86] Schwaab M, Pinto JC. Análise de Dados Experimentais I. 1st ed. Rio de Janeiro: 2007.
[87] Feng X, Li D, Chen J, Niu M, Liu X, Chan LLT, et al. Kinetic parameter estimation and simulation of trickle-bed reactor for hydrodesulfurization of whole fraction low-temperature coal tar. Fuel 2018;230:113–25.
[88] Chen T-M, Wang C-M, Wang I, Tsai T-C. Promoter effect of vanadia on Co/Mo/Al2O3 catalyst for deep hydrodesulfurization via the hydrogenation reaction pathway. J Catal 2010;272:28–36.
[89] Laredo GC, Altamirano E, Reyes JA de los. Self-inhibition observed during indole and o-ethylaniline hydrogenation in the presence of dibenzothiophene. Appl Catal A Gen 2003;242:311–20.
[90] Laredo S. GC, Reyes H. JA de L, Cano D. JL, Jesús Castillo MJ. Inhibition effects of nitrogen compounds on the hydrodesulfurization of dibenzothiophene. Appl Catal A Gen 2001;207:103–12.
[91] Lu M, Wang A, Li X, Duan X, Teng Y, Wang Y, et al. Hydrodenitrogenation of quinoline catalyzed by MCM-41-supported nickel phosphides. Energy and Fuels 2007;21:554–60. https://doi.org/10.1021/ef060467g.
[92] Braggio F de A, Mello MD de, Magalhães B da C, Zotin JL, Silva MAP da. Effects of citric acid addition method on the activity of NiMo/γ-Al2O3 catalysts in simultaneous hydrodesulfurization and hydrodenitrogenation reactions. Energy and Fuels 2019;33:1450–7.